

SN 2011ht: Confirming a Class of Interacting Supernovae with Plateau Light Curves (Type IIn-P)

Jon C. Mauerhan^{1*}, Nathan Smith¹, Jeffrey M. Silverman², Alexei V. Filippenko², Adam N. Morgan², S. Bradley Cenko², Mohan Ganeshalingam², Kelsey I. Clubb², Joshua S. Bloom², Thomas Matheson³, and Peter Milne¹

¹University of Arizona, Steward Observatory, Tucson, Arizona 85721, USA

²Department of Astronomy, University of California, Berkeley, CA 94720-3411, USA

³National Optical Astronomy Observatory, Tucson, AZ 85719, USA

18 September 2018

ABSTRACT

We present photometry and spectroscopy of the Type IIn supernova (SN) 2011ht, identified previously as a possible SN impostor. The light curve exhibits an abrupt transition from a well-defined ~ 120 day plateau to a steep bolometric decline, plummeting 4–5 mag in the optical and 2–3 mag in the infrared in only ~ 10 days. Leading up to peak brightness ($M_V = -17.4$ mag), a hot emission-line spectrum exhibits strong signs of interaction with circumstellar material (CSM), in the form of relatively narrow P-Cygni features of H I and He I superimposed on broad Lorentzian wings. For the latter half of the plateau phase, the spectrum exhibits strengthening P-Cygni profiles of Fe II, Ca II, and H α . By day 147, after the plateau has ended, the SN entered the nebular phase, heralded by the appearance of forbidden transitions of [O I], [O II], and [Ca II] over a weak continuum. At this stage, the light curve exhibits a low optical luminosity that is comparable to that of the most subluminous Type II-P supernovae, and a relatively fast visual wavelength decline that appeared to be significantly steeper than the ^{56}Co decay rate. However, the total pseudo-bolometric decline, including the infrared luminosity, is consistent with ^{56}Co decay, and implies a low ^{56}Ni mass in the range 0.006–0.01 M_\odot , near the lower end of the range exhibited by SNe II-P. We therefore characterize SN 2011ht as a core-collapse SN very similar to the peculiar SNe IIn 1994W and 2009kn. These three SNe appear to define a subclass, which are Type IIn based on their spectrum, but that also exhibit well-defined plateaus and produce low ^{56}Ni yields. We therefore suggest Type IIn-P as a name for this subclass. The absence of observational signatures of high-velocity material from SNe IIn-P could be the result of an opaque shell at the shocked SN-CSM interface, which remains optically thick longer than the time scale for the inner ejecta to cool and become transparent. Possible progenitors of SNe IIn-P, consistent with the available data, include 8–10 M_\odot stars, which undergo core collapse as a result of electron capture after a brief phase of enhanced mass loss, or more massive ($M \gtrsim 25 M_\odot$) progenitors, which experience substantial fallback of the metal-rich radioactive ejecta. In either case, the energy radiated by these three SNe during their plateau ($2\text{--}3 \times 10^{49}$ erg for SN 2011ht) must be dominated by CSM interaction, and the subluminous tail the result of low ^{56}Ni yield.

Key words: supernovae: general — supernovae: individual (SN 2011ht)

1 INTRODUCTION

Type IIn supernovae (SNe IIn) are a subset of core-collapse events that exhibit relatively narrow emission lines in their

spectra (Schlegel 1990; Filippenko 1997), indicating the presence of dense circumstellar material (CSM) that envelops the SN explosion (Chugai 1990). This CSM, which masks the broad emission and absorption features typically seen in normal SNe, must have been ejected by the progenitor in the years to decades prior to explosion. The enhanced

* E-mail: mauerhan@as.arizona.edu

mode of pre-SN mass loss can occur over a large range of time scales, from eruptive events months to years before the explosion, to long-duration superwinds that blow for millennia. As such, multi-epoch observations of SNe IIn allow us to probe the mass-loss parameters and physical states of massive stars immediately preceding their core collapse, providing a unique glimpse into the final phases of their evolution.

The progenitors of SNe IIn may span the entire range of massive-star classes, including luminous blue variables (LBVs; e.g., SN 2005gl, Gal-Yam & Leonard 2009; SN 2006tf, SN 2006gy, Smith et al. 2007, 2008; SN 1961V, Smith et al. 2011a, Kochanek et al. 2011; SN 2009ip, Mauerhan et al. 2012), red supergiants (RSGs; e.g., SN 2005ip, Smith et al. 2009; SN 1998S, Bowen et al. 2000, Mauerhan & Smith 2012), Wolf-Rayet stars (e.g., SN 1985F; Filippenko & Sargent 1985, Begelman & Sarazin 1986), as well as transitional Ofpe/WN9 stars on their way to the Wolf-Rayet phase (e.g., Smith et al. 2012a). Even the least massive of stars that are capable of becoming core-collapse SNe ($8\text{--}10 M_{\odot}$) might potentially generate a Type IIn explosion, a possibility considered in the case of the SN IIn 1994W (Sollerman et al. 1998). Thus, a diverse range of progenitors can potentially experience a highly enhanced degree of mass loss prior to exploding, but the time scales involved may vary significantly for evolved massive stars. Indeed, the physical mechanisms responsible for triggering the pre-SN superwinds and LBV eruptions are not understood. The fact that SNe IIn comprise only $\sim 9\%$ of all core-collapse events (Smith et al. 2011b; Li et al. 2011) complicates this picture, as there is no clear explanation why only a small fraction of massive stars spanning a large progenitor mass range experience such a highly enhanced degree of mass loss immediately before exploding.

For SNe IIn, the magnitude of the emission from CSM interaction is sensitive mainly to the velocity of the SN shock and the pre-SN wind density. These parameters can span a broad range, depending on the nature of the progenitor and its mass-loss history. It is thus difficult to gauge the magnitude of radioactive-element synthesis, or lack thereof, until after CSM interaction has diminished substantially. Some SNe IIn, such as the exceptionally luminous SN 2006gy, maintain powerful CSM interaction for so long that any radioactive-decay emission would fade away before becoming discernible in the light curve. Other interacting SNe, such as SNe 1980K and 1998S, reveal the common radioactive light-curve slope at earlier times, but still maintain enough CSM emission at late times to complicate or prevent radioactive diagnosis (e.g., Milisavljevic et al. 2012; Mauerhan & Smith 2012). Finally, a rare subset of SNe IIn that exhibit plateaus in their light curves, similar in shape to those of SNe II-P, become exceptionally faint after the plateau, well below the typical luminosity of radioactive decay. The SN IIn 1994W is of this latter subset, exhibiting an exceptionally faint and steeply declining light curve during its nebular phase, after a well-defined plateau.

Multiple interpretations have been considered in attempting to discern the peculiar properties of SN 1994W, including explosive pre-SN mass loss (Chugai et al. 2004) that was followed by an explosion having a low ^{56}Ni yield (Sollerman et al. 1998), as well as a non-SN interpretation of colliding stellar mass-loss shells (Dessart et al. 2009). Few SNe

have exhibited the unusual combination of observational properties displayed by SN 1994W. However, the SN IIn 2009kn was recently considered by Kankare et al. (2012) to be a “twin” of SN 1994W, based on the spectral morphology and a very similar well-defined plateau light curve. More recently, the discovery of SN 2011ht (Roming et al. 2011) has shown this SN to be an even closer twin of SN 1994W (Roming et al. 2012; Humphreys et al. 2012), exhibiting strikingly similar spectral evolution, a well-defined $\sim 110\text{--}120$ day plateau, and an exceptionally faint and steeply declining optical decay tail. In addition, the IIn SN 2005cl (Kiewe et al. 2012) shares the same spectral characteristics and well-defined plateau as SN 2011ht, SN 1994W, and SN 2009kn, although the plateau appears significantly more luminous. The late time luminosity of SN 2005cl was not constrained, however.

Soon after discovery, SN 2011ht was identified as an unusual object. Initially, it was classified by Roming et al. (2011, ATEL 3690) as a possible SN “impostor” — the eruption of an LBV. This explosion was one of the first to be observed in the UV band during the rise to peak, revealing an extreme UV brightening of ~ 7 mag, compared to ~ 2 mag in the optical, which probably resulted from shock-breakout photons degraded by diffusion through dense CSM. X-ray emission detected with *Swift* was also reported by Roming et al. (2012), although subsequent high-resolution X-ray imaging with *Chandra* revealed that this was likely to be a false match with a background X-ray source (Pooley 2012, ATEL 4062). The peak absolute visual magnitude of ~ -17 , and early spectral evolution led to the conclusion that SN 2011ht was perhaps a true SN IIn, not an impostor (Prieto et al. 2011, CBET 2903). In further support of this interpretation, the total radiated energy of 2.5×10^{49} erg derived for SN 2011ht during the first 110 days is far more luminous than typical LBV eruptions, unless the latter have a much wider luminosity distribution than currently thought (see Smith et al. 2011a). Still, Humphreys et al. (2012) have continued to favor the SN impostor hypothesis for SN 2011ht.

Here, we present photometric and spectroscopic observations of SN 2011ht. Based on the following analysis and comparison with SN 1994W, SN 2009kn, and, to a lesser extent, SN 2005cl, we interpret SN 2011ht as a true SN, and not a SN impostor. As such, it helps solidify a new class of interacting SNe that exhibit well-defined plateaus, spectra dominated by CSM interaction, and faint decay tails.

2 OBSERVATIONS

We began photometric monitoring of SN 2011ht roughly 28 days after its discovery date of 2011 Sep. 29. We obtained optical *BVRI* photometry using the 1 m Nickel telescope at Lick Observatory, and infrared (IR) *JHK* photometry using the 1.3 m Peters Automated Infrared Imaging Telescope (PAIRITEL)¹ on Mt. Hopkins (Bloom et al. 2006). The photometric measurements were obtained over 17–19 separate epochs between days 28–150 after discovery. Late-time photometry on days 203 and 221 was also obtained using the 90Prime Imager on the Bok 90” telescope on Kitt Peak, and

¹ See <http://www.pairitel.org/>.

Table 1. Optical photometry of SN 2011ht. Epochs are given with respect to discovery date (2011 Sep. 29). The uncertainties represent the standard deviation of the zero-point magnitudes derived from measurements of 4–5 field stars.

JD–2,450,000 /Epoch (days)	<i>B</i> (mag)	<i>V</i> (mag)	<i>R</i> (mag)	<i>I</i> (mag)
5868.8/35	14.41(0.05)	14.46(0.14)	14.23(0.09)	14.18(0.08)
5873.8/40	14.32(0.05)	14.37(0.14)	14.15(0.09)	14.08(0.07)
5875.8/42	14.26(0.06)	14.38(0.15)	14.16(0.12)	14.13(0.11)
5879.5/46	14.28(0.05)	14.35(0.15)	14.15(0.13)	14.14(0.15)
5888.8/55	14.50(0.10)	14.26(0.17)	14.17(0.14)	14.16(0.14)
5893.5/60	14.37(0.06)	14.45(0.21)	14.24(0.18)	14.18(0.17)
5898.5/65	14.51(0.06)	14.59(0.21)	14.39(0.19)	14.21(0.21)
5901.5/68	14.52(0.06)	14.57(0.21)	14.34(0.17)	14.23(0.17)
5905.5/72	14.60(0.06)	14.64(0.21)	14.32(0.15)	14.24(0.17)
5912.5/79	14.71(0.05)	14.69(0.15)	14.46(0.14)	14.35(0.13)
5924.8/91	15.07(0.06)	14.95(0.21)	14.68(0.19)	14.52(0.20)
5933.5/100	15.46(0.04)	15.20(0.20)	14.85(0.20)	14.78(0.21)
5936.5/103	15.51(0.06)	15.23(0.21)	14.91(0.19)	14.69(0.19)
5943.5/110	15.80(0.06)	15.35(0.21)	15.03(0.19)	14.79(0.20)
5957.8/124	16.68(0.05)	15.88(0.15)	15.37(0.11)	15.03(0.12)
5961.5/128	17.38(0.06)	16.49(0.21)	15.94(0.19)	15.55(0.18)
5974.5/141	20.39(0.21)	19.96(0.20)	19.11(0.20)	18.48(0.21)
6036.5/203	...	21.39(0.25)	20.77(0.20)	20.37(0.15)
6054.6/221	21.43(0.15)	...

Table 2. PAIRITEL near-IR photometry of SN 2011ht. The uncertainties are statistical.

JD–2,450,000 /Epoch (days)	<i>J</i> (mag)	<i>H</i> (mag)	<i>K</i> (mag)
5861.5/28	14.23(0.03)	13.97(0.05)	13.72(0.08)
5864.5/31	14.05(0.02)	13.86(0.03)	13.61(0.06)
5866.5/33	14.00(0.02)	13.88(0.03)	13.67(0.09)
5882.5/49	13.92(0.02)	13.78(0.03)	13.51(0.05)
5888.4/55	13.89(0.02)	13.68(0.03)	13.43(0.05)
5892.4/59	13.88(0.03)	13.70(0.05)	13.62(0.09)
5894.4/61	13.86(0.02)	13.70(0.03)	13.48(0.07)
5900.5/67	13.94(0.02)	13.75(0.03)	13.62(0.04)
5903.5/70	13.94(0.02)	13.77(0.02)	13.54(0.04)
5922.4/89	14.09(0.02)	13.94(0.03)	13.65(0.06)
5928.4/95	14.11(0.02)	13.92(0.02)	13.63(0.06)
5932.4/99	14.17(0.02)	13.94(0.03)	13.70(0.06)
5936.4/103	14.21(0.03)	13.94(0.05)	13.82(0.14)
5949.4/116	14.34(0.02)	14.07(0.03)	13.83(0.06)
5953.4/120	14.33(0.02)	14.10(0.05)	13.97(0.09)
5959.4/126	14.66(0.02)	14.37(0.03)	14.17(0.06)
5961.4/128	15.01(0.06)	14.76(0.11)	14.61(0.23)
5964.3/131	16.04(0.07)	15.45(0.09)	...
5966.3/133	16.79(0.07)	16.59(0.12)	...
5968.4/135	16.77(0.10)
5977.4/144	18.28(0.25)	17.03(0.20)	16.28(0.2)

the MONT4K Imager on the Kuiper 61'' telescope on Mt. Bigelow, respectively. A MONT4K image of the SN is shown in Figure 1. The Lick and PAIRITEL photometry was extracted using standard aperture-photometry techniques and calibrated by photometry of 4–6 field stars in the same image as the SN, while the late-time 90Prime and MONT4K photometry was extracted via point-spread-function (PSF) fitting with the IDL Starfinder code, in which case the host galaxy was modeled as local background, allowing for a more precise determination of the faint SN flux. Tables 1 and 2 list the results.

Our spectroscopic monitoring campaign of SN 2011ht utilized the Kast spectrograph (Miller & Stone 1993) on the 3 m Shane reflector at Lick Observatory, the Low Resolution Imaging Spectrometer (LRIS; Oke et al. 1995) on the Keck

Table 3. Spectroscopic observations of SN 2011ht

JD–2,450,000 /Epoch (days)	Facility	Coverage (Å)	<i>R</i> $\delta\lambda/\lambda$
5860/26	Lick/Kast	3436–9920	1400, 900
5867/33	Keck/LRIS	3362–5630	1400
5867/33	Keck/LRIS	5740–7390	2200
5892/58	Lick/Kast	3436–9920	1400, 900
5898/64	Keck/LRIS	3362–5630	1400
5898/64	Keck/LRIS	5740–7390	2200
5914/80	Lick/Kast	3436–9920	1400, 900
5921/88	Keck/LRIS	3362–5630	1400
5921/88	Keck/LRIS	5740–7390	2200
5922/89	Lick/Kast	3436–9920	1400, 900
5928/96	MMT/BlueCh	5550–7500	4500
5929/96	Lick/Kast	3436–9920	1400, 900
5944/111	Lick/Kast	3436–9920	1400, 900
5946/113	MMT/BlueCh	5550–7500	4500
5956/123	MMT/BlueCh	5550–7500	4500
5958/125	Lick/Kast	3436–9920	1400, 900
5961/127	KPNO/RCSpec	3600–8270	1100
5981/147	Lick/Kast	3436–9920	1400, 900
5981/147	Keck/LRIS	3362–5630	1400
5981/147	Keck/LRIS	5740–7390	2200
5988/155	MMT/BlueCh	5550–7500	4500
6034/201	MMT/BlueCh	3920–8998	500
6036/202	Lick/Kast	3436–9920	1400, 900
6046/213	Keck/LRIS	5740–7390	2200
6071/238	MMT/BlueCh	5550–7500	4500

I 10 m telescope, the Bluechannel spectrograph on the Multiple Mirror Telescope (MMT), and the RC Spectrograph (RCSpec²) on the Mayall 4 m reflector at Kitt Peak National Observatory (KPNO). The spectroscopic observations are summarized in Table 3. The Lick/Kast spectra have moderate resolution ($R \equiv \delta\lambda/\lambda \approx 900$ and 1400 for the red and blue sides of the Kast spectra, respectively) and covered a large wavelength range of 3436–9920 Å. The Keck/LRIS and MMT/Bluechannel spectra have higher spectral resolving power of $R \sim 2200$ and 4500, respectively. The RC-Spec spectra cover a wavelength range of 3200–8270 Å with a spectral resolving power of ~ 1100 . All spectra were generally obtained at low airmass or with an atmospheric dispersion corrector; otherwise, observations were performed with the slit at the parallactic angle in order to minimize chromatic differential slit losses (Filippenko 1982). Our data reduction, wavelength and flux calibration followed standard techniques as described by Silverman et al. (2012). Lick/Kast spectra of SN 2009kn, acquired and reduced utilizing the same instruments setting and reduction techniques described above, were also obtained on 2009 Nov. 10 and Dec. 9. Finally, we also reproduce spectra of SN 1994W, originally presented in Chugai et al. (2004).

3 RESULTS

3.1 The Light Curve

The optical and IR light curves of SN 2011ht are presented in Figure 2. The first 20–30 days of monitoring cover the rise to maximum light followed by an extended 120-day plateau phase. The optical light curves peak near day 45 and the IR curves peak approximately two weeks later, near day 60. Between days 60 and 120, the optical curves begin a shallow

² <http://www.noao.edu/kpno/manuals/rcspec/rcsp.html>

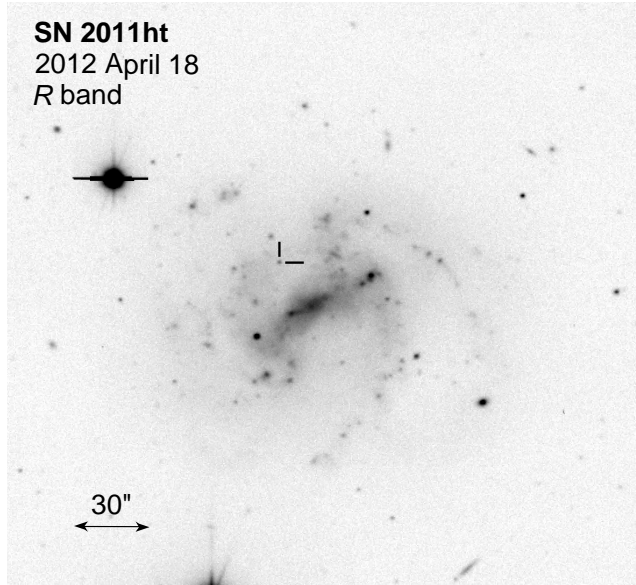


Figure 1. *R*-band image of UGC 4560 and SN 2011ht obtained with the 90Prime Imager on 2012 April 18 when the SN was at $R = 20.77$ mag. North is up and east to the left.

decline that steepens with decreasing wavelength. In the *B* band, the curve gradually drops ~ 2 mag before the end of the plateau on day ~ 120 , while the *JHK* curves maintain relatively constant brightness for the duration of the plateau. By day 130, the light curve has begun a rapid descent of 4–5 mag in the optical and 2–3 mag in the infrared over a time scale of ~ 10 days. By day ~ 140 , a floor has been reached and the light curves subsequently exhibit a steady decline that continues through at least day 221.

The color curves at the bottom of Figure 2 illustrate the gradual intrinsic reddening of the SN during the plateau phase, as the flux at shorter wavelengths decreases the fastest. Once the plateau phase has ended, the optical colors (including $V - I$) flatten out, becoming slightly bluer. However, there is a substantial shift of flux toward the IR during the nebular phase, as evidenced by the continually increasing $V - H$ and $V - K$ curves. SN 2009kn and SN 1994W exhibit similar color trends in the optical and IR (Kankare et al. 2012), although the late-time IR coverage is not as complete as it is for SN 2011ht.

We computed the absolute magnitude of SN 2011ht, adopting an extinction value of $A_V = 0.19$ mag and a distance of 19.2 Mpc to the host galaxy UGC 5460 (Roming et al. 2012), which yielded values of $M_V = -17.35$ and $M_R = -17.41$ mag at the respective peaks of days 55 and 46. The absolute magnitude light curve of SN 2011ht is presented in Figure 3, along with the those of various other core-collapse SNe and a SN impostor for comparison. The well-defined steep-edge plateau of SN 2011ht closely resembles that of the SNe IIn 2009kn, SN 2005cl, and SN 1994W, although the plateau peaks of SN 1994W and SN 2005cl appeared up to 1.5–2 mag brighter. The plateaus of each have similar durations of ~ 110 –120 days and subsequently drop by a comparable magnitude. Plateaus with edges this steep are not a typical characteristic of SNe IIn. However, the plateau durations are very similar to normal SNe II-P (Hamuy 2003). The subsequent decay tails of these SNe are

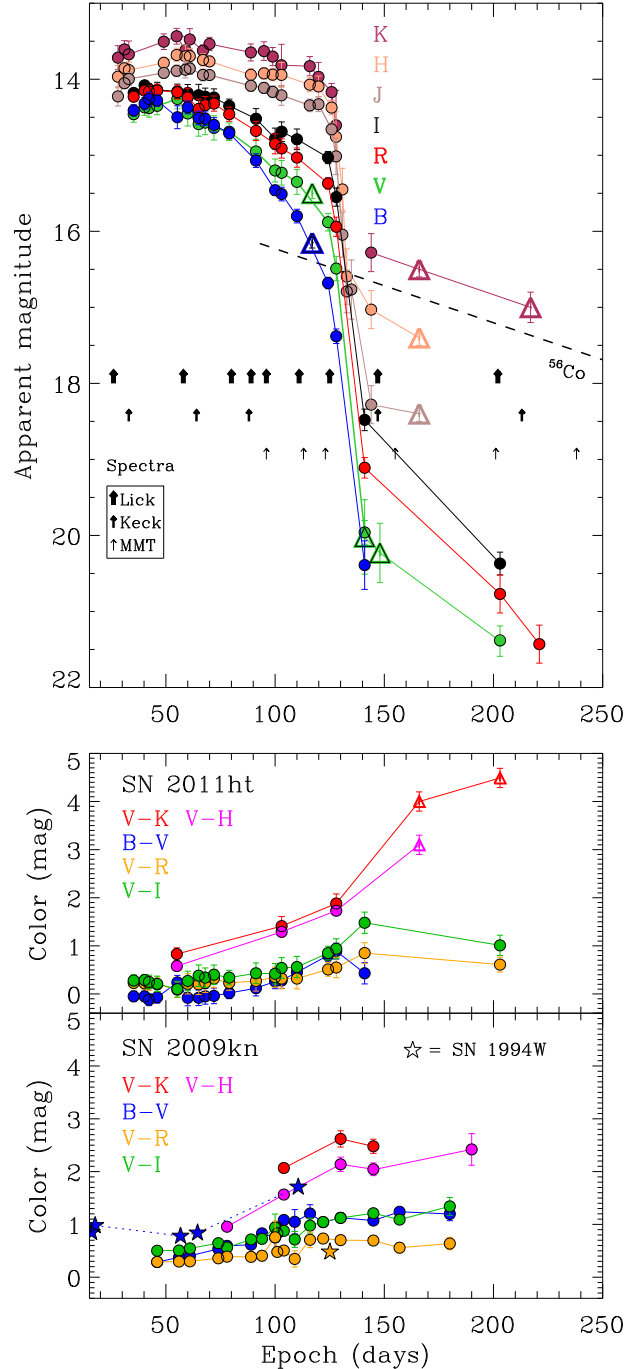


Figure 2. *BVRIJHK* light and color curves of SN 2011ht, with supplemental data from Humphreys et al. (2012; *triangles*). The color curves of SN 2009kn and SN 1994W (from Kankare et al. 2012) have been included for comparison. Epochs having accompanying spectra are marked with upward arrows. The dashed line exhibits the decline rate of ^{56}Co decay, for an arbitrary ^{56}Ni mass.

relatively faint for SNe IIn, but lie near the lower end of the range exhibited by SNe II-P (Nadyozhin 2003; Smartt et al. 2009). The optical decline rates of SN 2011ht and SN 1994W are also relatively steep, at 0.03 – 0.05 mag day $^{-1}$. This behavior is rather uncharacteristic of normal SNe II-P, perhaps more similar to H-deficient SNe Ib/c, which typically exhibit

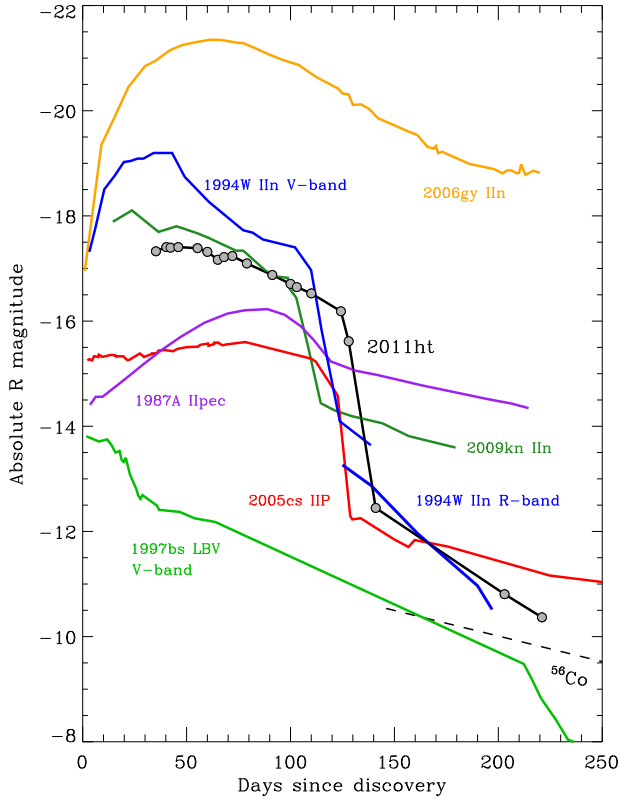


Figure 3. Absolute light curve of SN 2011ht, including comparison SNe 1994W (IIn; Sollerman et al. 1998), 2009kn (IIn; Kankare et al. 2012), 2005cl (Kiewe et al. 2012); 2005cs (II-P, Pastorello et al. 2009), 1987A (II-pec, Hamuy et al. 1990), and 2006gy (Smith et al. 2007), as well as LBV SN “impostor” 1997bs (Van Dyk et al. 2000). The height of the SN 2011ht plateau is typical of SNe IIn, but the late-time tail appears significantly subluminous and declines at a relatively rapid rate, like SN 1994W. The dashed line exhibits the decline rate of ^{56}Co decay, for an arbitrary ^{56}Ni mass.

faster decline rates of $0.01\text{--}0.02\text{ mag day}^{-1}$ (Elmhamdi et al. 2011); still, SNe 2011ht and 1994W decline substantially more rapidly than even those objects, in the optical.

We also derived a pseudo-bolometric luminosity for SN 2011ht. For the plateau phase we calculated bolometric corrections using our measured optical colors in conjunction with the method described by Bersten & Hamuy (2009), which is valid only for the plateau. Using the extinction-corrected $B - V$ and $V - I$ colors, two independent values of pseudo-bolometric luminosity were computed for every epoch during the plateau and the results were averaged. The average difference between the two color-dependent luminosity values over all epochs was 0.36 dex. The rather large discrepancy probably results from the fact that this method was derived for SNe II-P, specifically, which generally have redder intrinsic colors than SNe IIn. Thus, we also calculated the pseudo-bolometric luminosity by integrating the source spectral energy distribution (SED) between the B and K bands, using trapezoidal integration. The resulting peak luminosity near day 55 is $L_{\text{peak}} \approx 2 \times 10^{42}\text{ erg s}^{-1}$,

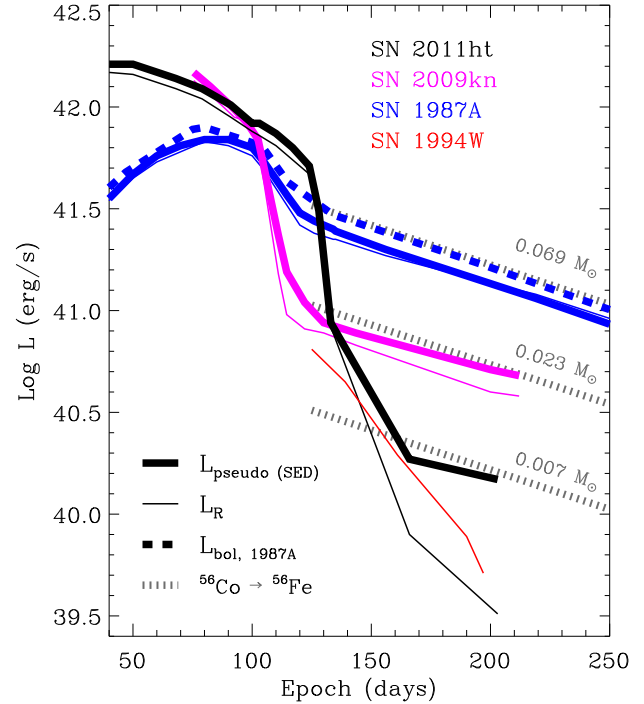


Figure 4. Pseudo-bolometric (thick lines) and R -band (thin lines) luminosity light curves of SN 2011ht (black), SN 2009kn (red), and SN 1987A for comparison (blue). The pseudo-bolometric curves were derived by integrating the SEDs of both SNe between the B and K bands. For SN 1987A, this method underestimates the true bolometric luminosity by nearly 20%, so we assume that this is a reasonable estimate for the error in our pseudo-bolometric curves. In the case of SN 2011ht, the slope of the late-time pseudo-bolometric tail is consistent with the rate of ^{56}Co decay (dashed lines), even though the individual R -band tail is not. The result suggests that the unusually steep late-time decline in the optical could be the result of flux shifting to longer wavelengths at late times. The ^{56}Co decay curves are shown for several values of ^{56}Ni mass.

which is slightly below the peak bolometric luminosity reported by Roming et al. (2012), probably because we have not accounted for the U -band optical and UV flux, which is significant. We then computed the total radiated energy of the plateau again using trapezoidal integration on the light curve, which yielded a total energy of $E_{\text{rad,p}} \approx 2 \times 10^{49}\text{ erg}$. Again, since this method did not account for the luminosity blueward of B band and redward of K band, it could be considered a lower limit. Nonetheless, the value is high, much higher than that of most SN impostors (Smith et al. 2011a), although normal for core-collapse SNe.

Although the post-plateau optical decline of SN 2011ht is unusually steep, the available K -band measurements during this phase (from Humphreys et al. 2012), also shown in Figure 2, appear to be consistent with the ^{56}Co decay rate. The much smaller drop in brightness for the IR after the plateau suggests that a substantial amount of optical flux has shifted to longer wavelengths. So, to obtain a more accurate estimate of the post-plateau pseudo-bolometric luminosity of SN 2011ht, we, again, integrated their extinction-corrected SEDs between the B and K bands. To match

the available IR post-plateau data for SN 2011ht from Humphreys et al. (2012) on day 166, we estimated the optical photometry of SN 2011ht by linearly interpolating between our measured points on days 141 and 203. For epoch 203, for which we have secure *VRI* detections, we interpolated the *K*-band photometry along the line connecting the measurements on days 166 and 217 from Humphreys et al. (2012). The pseudo-bolometric curves of SN 2009kn were computed in the same way, adopting measurements from Kankare et al. (2012). Finally, we also performed the same SED integration for SN 1987A, using photometric data from the literature (Menziez et al. 1987; Catchpole et al. 1987, 1988), sampling only a small fraction of the available data to match our cadence of SN 2011ht; and we compared this result with the true bolometric luminosity curve from Bouchet et al. (1991).

The resulting pseudo-bolometric light curves of SN 2011ht, SN 2009kn, and SN 1987A are presented in Figure 4, along with the absolute *R*-band curves for comparison. Without a priori knowledge of the full SED, we are unable to quantify how much flux remains unaccounted for at wavelengths shorter than *B* band or longer than *K* band. Hence, the uncertainties in our luminosity calculations are difficult to ascertain. Some guidance may be provided by application of our SED-integration method to SN 1987A, whose true bolometric luminosity is well constrained. In this case, the true bolometric luminosities are only marginally higher than our pseudo-bolometric values during the plateau phase ($\approx 5\%$), while they are $\approx 20\%$ higher during the post-plateau decay tail, likely as a result of the unaccounted flux outside of the *B*-band to *K*-band range we considered. Still, the shape of the light curves and the decline rate remains consistent between the true bolometric and pseudo-bolometric values of SN 1987A, which is reassuring.

Although the *optical* decay tail of SN 2011ht suggests a decline rate faster than the rate of ^{56}Co decay, the pseudo-bolometric luminosity, which includes the near-IR flux, declines at a rate consistent with ^{56}Co decay. The decay of tail SN 2011ht is relatively faint, however, compared with known SNe II_n, perhaps because many of them continue strong CSM interaction into late phases. In any case, the late time luminosity of SN 2011ht lies near the lower end of the range exhibited by SNe II-P (Nadyozhin 2003; Smartt et al. 2009), which suggests a relatively low mass of ^{56}Ni . Overall, the behavior of SN 2011ht, like SN 2009kn, appears consistent with that of a bona fide core-collapse SN.

3.2 Spectral Evolution

Our Lick/Kast spectra of SN 2011ht and SN 2009kn are presented in Figure 5, in addition to three later epochs of SN 2009kn from Kankare et al. (2012), and archival spectra of SN 1994W from Chugai et al. (2004). Spectra of SN 2005cl are also included for comparison, and were obtained from the Weizmann interactive SN data repository (Yaron & Gal-Yam 2012). Figure 6 shows our higher-resolution spectra from Keck/LRIS and KPNO/RCSpec. Figure 7 displays the same Keck/LRIS spectra, in addition to our MMT spectra, all centered on the $\text{H}\alpha$ emission line. During our earliest epoch on day 26, SN 2011ht exhibits a characteristic SN II_n emission-line spectrum, dominated by the Balmer series of H I. The emission lines exhibit intermediate-width

cores of full width at half-maximum intensity (FWHM) $\sim 1500 \text{ km s}^{-1}$ on top of broad Lorentzian wings, which presumably form as a result of Thomson scattering of photons off of free electrons in the dense CSM and within the post-shock gas (Chugai et al. 2001; Dessart et al. 2009). The $\text{H}\alpha$ emission profile is slightly asymmetric, having a more extended red wing. The underlying broad components have full-width near zero intensity (FWZI) values of $8000\text{--}9000 \text{ km s}^{-1}$ on day 33, and weaken to $\sim 7000 \text{ km s}^{-1}$ by day 64. The lines exhibit narrow P-Cygni absorption components with blueshifted velocities of $\sim 500\text{--}600 \text{ km s}^{-1}$, which remain at roughly constant velocity throughout the entire plateau phase. Weak emission from He I $\lambda 5876$ is present at the earliest epochs and strongest on day 58. Weak absorption features of Fe II and Ca II H&K are present by day 80, in addition to weak Mg II $\lambda 7888$ in pure emission. By day 58 (when the light curve is near maximum) the spectrum has increased in ionization temperature, with the strengthening of He I $\lambda 5876$ and the appearance of He I $\lambda 7065$, in addition to the development of a strong blue excess that rises shortward of 5500 \AA . The excess becomes apparent near a cluster of Fe II lines, which become individually distinguishable as absorption-dominated P-Cygni features by day 80 and are accompanied by additional absorption features of this species in between $\text{H}\beta$ and $\text{H}\gamma$. Redward of this bump the slope of the continuum appears to be consistent with a $10,000 \text{ K}$ blackbody.

The Balmer lines and Fe II P-Cygni features appear in greater detail in our higher-resolution spectra (Fig. 6), revealing that the Fe II lines also exhibit signs of Lorentzian broadening. Thus, the blue excess from day 58 appears to be the result of blended Fe II emission features, like SN 2005ip (Smith et al. 2009) and SN 2006jc (Chugai 2009; Foley et al. 2007).

On day 89 (for all SNe, the day is given with respect to the discovery date) the spectrum has begun to exhibit the characteristics of a cool, dense gas, very similar to SN 1994W on day 58 and SN 2009kn on day 59. Continuously strengthening Fe II features are accompanied by P-Cygni lines of the Ca II triplet at $7500\text{--}8000 \text{ \AA}$, all of which continue to increase in strength through days 125–127, at which point Na I P-Cygni and absorption features also become evident. By this time, the continuum temperature has decreased to $\sim 6200 \text{ K}$, and the broad Lorentzian wings of $\text{H}\alpha$ have become diminished beyond detectability, as evidenced by the higher-resolution spectra of $\text{H}\alpha$ shown in Figure 7. In addition, line blanketing suppresses the flux at the blue end of the spectrum, which must be partially responsible for the greater drop in the *B*-band light curve in Figure 2 (in addition to a decrease in blackbody temperature), before the plateau edge has been reached.

By the time of the spectrum on day 147, the light curve exhibits a steady decline, the continuum has weakened substantially, and the P-Cygni profiles are less prominent. The higher-resolution $\text{H}\alpha$ spectrum in Figure 7, however, shows that P-Cygni absorption is still present. The Balmer series has weakened significantly, with only $\text{H}\alpha$, $\text{H}\beta$, and $\text{H}\gamma$ clearly visible. Forbidden transitions of [O I], [O II], and [Ca II] have also appeared, the latter of which implies very low density for the gas. These features imply that the SN has entered the nebular phase. All emission lines remain narrow

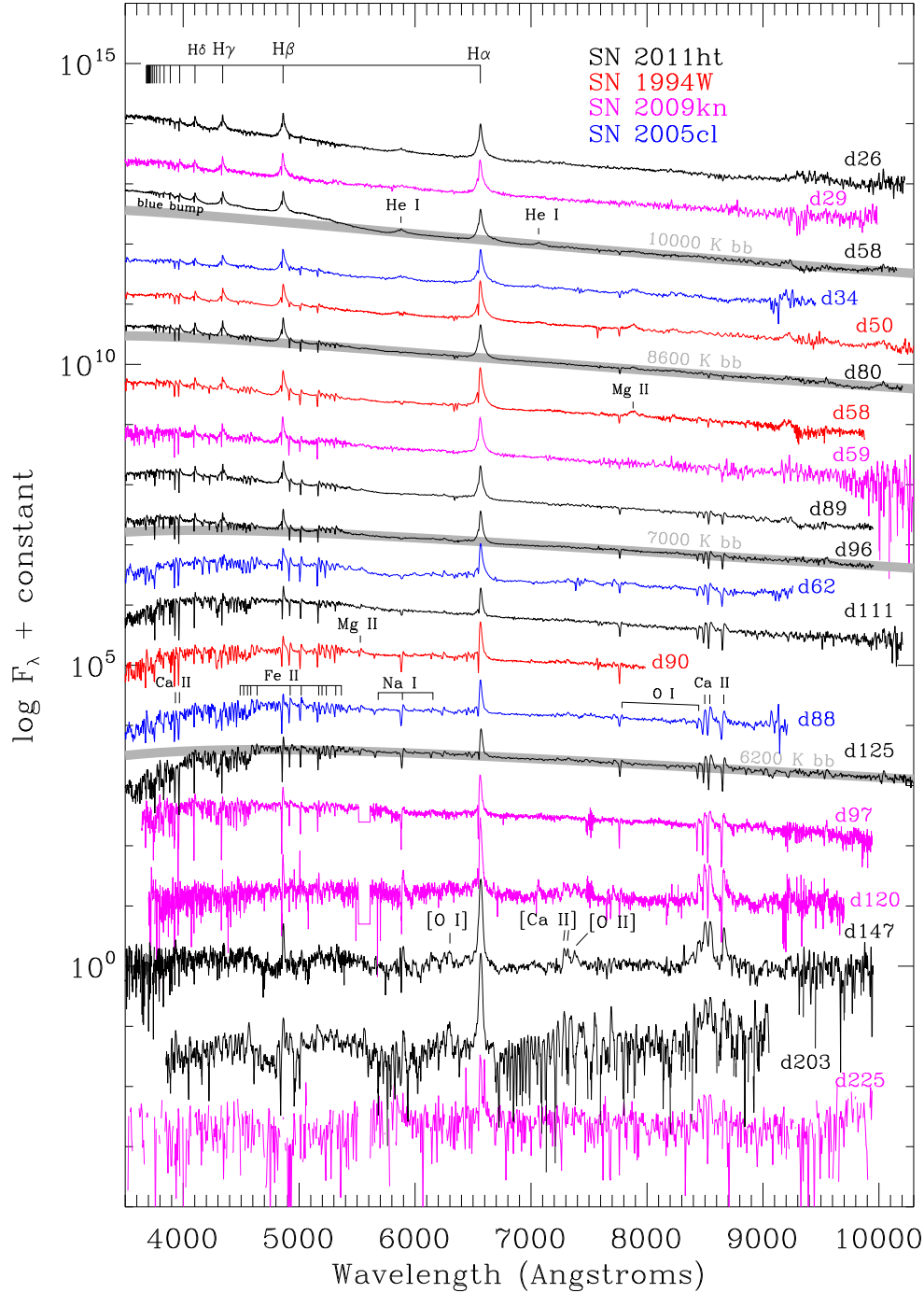


Figure 5. Dereddened spectra of SN 2011ht and its kin: SN 1994W (red), SN 2009kn (magenta), and SN 2005cl (blue). The SN 2005cl spectra were obtained from the Weizmann interactive SN data repository (Yaron & Gal-Yam 2012). Our own SN 2009kn spectra for days 29 and 59 are supplemented with spectra from days 97, 120, and 225 (Kankare et al. 2012), kindly provided by E. Kankare.

(< 1200 km s⁻¹) throughout our spectroscopic coverage of this phase.

Using the distance and extinction values that we adopted to generate the absolute-magnitude curve in Figure 3, we calculated the luminosities of the H α and H β emission lines, and compared them with those of SN 1994W

(data from Chugai et al. 2004) and SN 2009kn (Kankare et al. 2012). The same measurements were made for SN 2005cl, adopting the distance and extinction values from (Kiewe et al. 2012). The results are presented in Figure 8. SN 1994W and SN 2005cl have a substantially higher H α luminosity than SN 2011ht and SN 2009kn during the plateau phase,

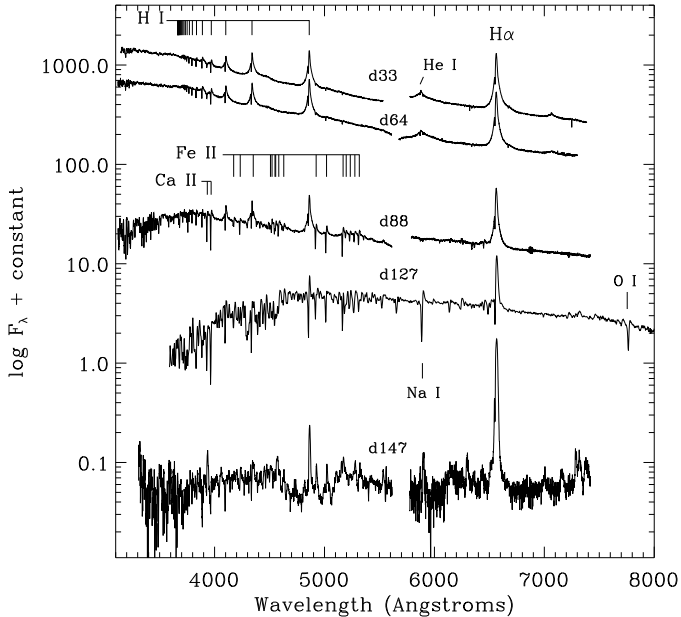


Figure 6. Optical spectra of SN 2011ht from Keck/LRIS, and a KPNO/RCSpec spectrum from day 127.

by almost an order of magnitude, which could be the result of interaction with higher-density CSM, a different CSM filling factor (i.e., clumping), or geometric differences. After their plateau phases end around ~ 120 days, the light curves of each SN converge to the same late-time $H\alpha$ luminosity. The $H\alpha$ decline rates of SN 2011ht and SN 1994W are identical throughout their nebular phases, and are steeper than SN 2009kn. Nebular phase coverage is not available for SN 2005cl, however. The fact that the line emission does not exhibit the same sharp plateau edge as the broad-band light curves of these SNe suggests that the continuum and $H\alpha$ emission source might not be coupled.

After the plateau, $H\beta$ becomes noticeably fainter than $H\alpha$ for each SN, corresponding to a change in Balmer decrement. During the remainder of the nebular phase, $H\beta$ exhibits approximately steady decline, somewhat steeper than for $H\alpha$.

4 DISCUSSION

SNe 2011ht, 1994W, and 2009kn share an unusual set of properties, particularly the combination of a luminous well-defined plateau light curve, a faint decay tail, and nearly identical spectral evolution that is distinct from the larger class of SNe IIn. SN 2005cl exhibits similar characteristics, although the lack of post-plateau information limits the comparison of this SN to the former group. The unique character of these SNe suggests that a very specific physical scenario has played out in each of these events, involving circumstellar interaction and low ^{56}Ni yield. It therefore appears plausible that the same type of explosion has taken place in each case, whatever the underlying physics might be. Various possibilities, consistent with the available data, are discussed below.

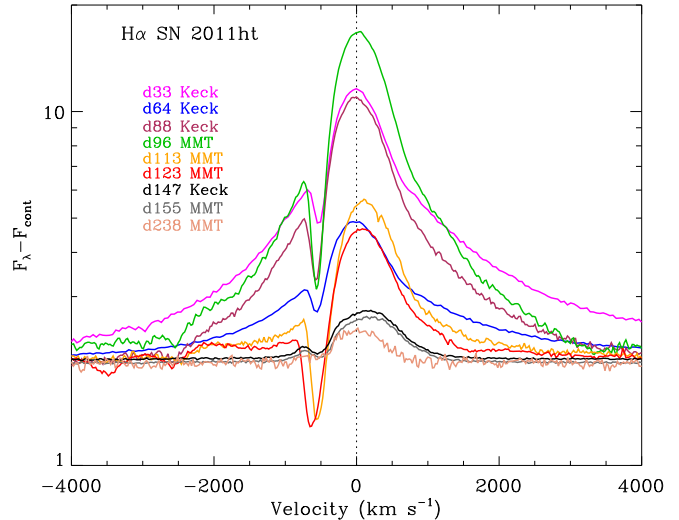


Figure 7. Evolution of the continuum-subtracted $H\alpha$ profile of SN 2011ht between days 33 and 238 after discovery. At early times, the emission line exhibits an intermediate-width ($\sim 1500 \text{ km s}^{-1}$) core P-Cygni profile with superimposed broad Lorentzian wings. At later times, the wings diminish, yet P-Cygni absorption remains present well into the nebular phase.

4.1 Circumstellar Interaction

The photometric and spectroscopic evolution of SN 2011ht during the plateau phase, specifically the high luminosity and the relatively narrow P-Cygni emission-line profiles superimposed on the broad Lorentzian wings, indicates strong interaction with CSM. SN 1994W exhibited a nearly identical spectral morphology and evolution, and modeling of this SN by Chugai et al. (2004) demonstrated that homologous expansion of dense CSM is required to fit the observational data. Additional modeling of this SN by Dessart et al. (2009) resulted in different conclusions about the origin of the spectral features, but also found that CSM interaction produced a good match to the spectrum.

The Chugai et al. (2004) model concluded that the CSM of SN 1994W consists of a $0.4 M_{\odot}$ envelope having an accelerated velocity gradient of $170\text{--}400 \text{ km s}^{-1}$ within a radius of $3.3 \times 10^{15} \text{ cm}$, which implies a very high mass-loss rate of $0.3 M_{\odot} \text{ yr}^{-1}$ that probably occurred $\sim 1.5 \text{ yr}$ before core collapse. Such a large mass-loss rate is beyond the physical parameters of a sustainable line-driven stellar wind, and implies an eruptive/explosive origin for the CSM (Smith & Owocki 2006). The observational characteristics of SNe 2011ht and 2009kn, and perhaps SN 2005cl, are so similar to those of SN 1994W that one could reasonably arrive at a similar physical interpretation for these SNe.

Figure 9 shows the best-fit model light curves for SN 1994W from Chugai et al. (2004) — specifically, their model “sn94w43”. To match the SN 2011ht data, we shifted the SN 1994W models down by a factor of 6–7 in luminosity ($\sim 2 \text{ mag}$) and forward in time by 16 days (perhaps accounting for uncertainties in the explosion dates). For the R and V bands, the model plateau shape and the abrupt transition into the tail phase matches the SN 2011ht photometric data well, although the match to the B -band plateau data is not as satisfactory for the latter half of the plateau.

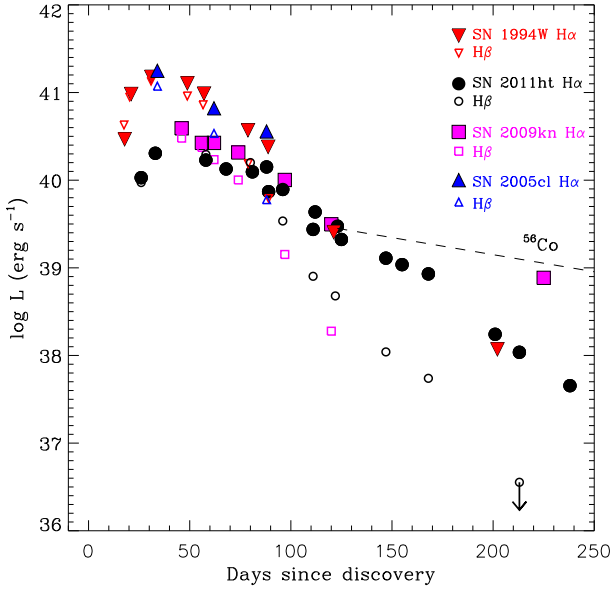


Figure 8. Light curves of H α and H β luminosity for SNe 2011ht, 1994W, 2009kn, and 2005cl. All objects exhibit very similar luminosity evolution and, in cases where late-time data are available, a steep late-time decline that is faster than the rate of ^{56}Co decay. SN 1994W and 2005cl are relatively luminous during their plateau phases, although each object having late-time coverage converges to the same post-plateau H α luminosity around day 120. The late-time declines of SNe 2011ht and 1994W are identical, at least out to day 203.

The SN 2011ht data match the overall shape of the SN 1994W model light curve, but the factor of 6–7 discrepancy in peak H α luminosity must be accounted for. Assuming strong interaction between a SN shock and surrounding CSM during the plateau phase, the luminosity of H α can be expressed as

$$L(\text{H}\alpha) \propto \frac{L_s}{T_s} \propto \frac{V_s^3}{T_s} \left(\frac{\dot{M}}{v_w} \right), \quad (1)$$

where L_s , T_s , and V_s are the shock ionizing luminosity, temperature, and velocity (respectively), and $w = \dot{M}/v_w$ is the wind-density parameter. For SN 1994W, Chugai et al. (2004) estimated the shock velocity to be 4000 km s^{-1} and the shock temperature to be within a reasonable range of $1\text{--}2 \times 10^4 \text{ K}$. Their model, which requires a $0.3 M_\odot \text{ yr}^{-1}$ mass-loss rate and 400 km s^{-1} wind velocity, implies a very high wind-density parameter. Because of the high sensitivity of H α emission to shock velocity, a factor of less than 2 difference in V_s alone could account for the factor of 6–7 lower luminosity of H α , assuming the CSM wind-density parameters were similar for SN 2011ht and SN 1994W. This could be achievable by either an intrinsically faster shock, or a bigger velocity difference between the shock and the expanding CSM. Alternatively, if the shock velocities (and temperatures) are the same, which is supported by the very similar plateau durations, then the luminosity differences could instead indicate a lower-density CSM, or a lower geometric covering factor (solid angle) associated with the CSM of SN 2011ht. Assuming that differences in the CSM velocity between SN 2011ht and SN 1994W could be traced approx-

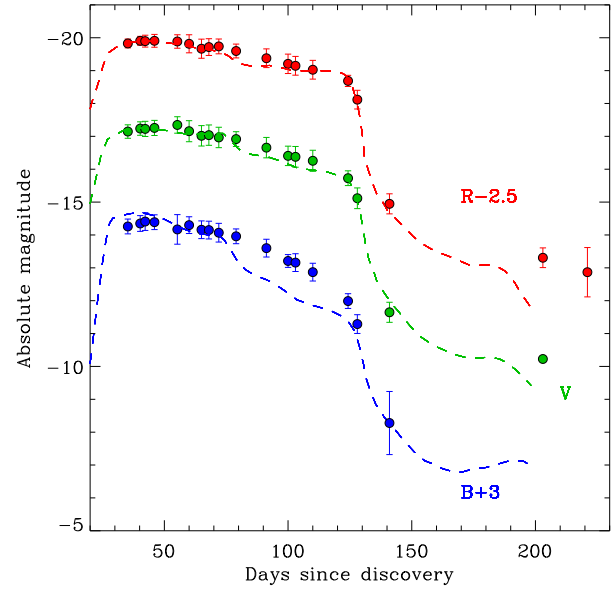


Figure 9. BVR light curves of SN 2011ht plotted against a scaled CSM-interaction light-curve model for the SN II in 1994W from Chugai et al. (2004).

imately by the relative blueshifts of their H α P-Cygni absorption components, then the factor of 1.5 smaller blueshift for SN 2011ht would imply a factor of ~ 1.5 increase in H α luminosity. The fact that H α is nearly an order of magnitude fainter for SN 2011ht during the plateau thus requires an order of magnitude lower mass-loss rate for the progenitor, or $0.03 M_\odot \text{ yr}^{-1}$. This value is still extremely high, however, and thus would also imply an eruptive/explosive origin for the CSM associated with SN 2011ht.

The luminosity and decline rate of H α during the nebular phase is practically identical for SN 2011ht and SN 1994W. In the latter case, Chugai et al. (2004) used the late-time H α luminosity to constrain the outer pre-eruption wind parameters of the progenitor. The low luminosity of SN 1994W on day 203 ($L \approx 10^{38} \text{ erg s}^{-1}$) implies that the outer wind should have a density ~ 10 and ~ 2 times lower than that of the well-studied SN 1979C and SN 1980K (respectively), which presumably had red-supergiant progenitors (Fesen & Becker 1990; Weiler et al. 1991). The dramatic change in mass-loss rate supports the hypothesis of eruptive/explosive mass loss several years preceding the SN. Again, owing to the striking similarities shared with SN 1994W, both qualitatively and quantitatively, one arrives at a similar conclusion for the outer-wind parameters of SN 2011ht.

The very steep plateau edges in the light curves of SNe 2011ht, 1994W, 2009kn, and 2005cl are rather unusual for SNe II, which normally exhibit a slower and more steady decline. In the case of SN 1994W, Chugai et al. (2004) interpreted this characteristic as the result of the SN shock wave reaching the edge of a dense CSM envelope, while Dessart et al. (2009) favored simple photospheric contraction as a result of hydrogen cooling to recombination temperature. The latter scenario was also favored by Kankare et al. (2012) in the case of SN 2009kn. However, both of these scenarios

could play a role in producing the sharp plateau edge. As the SN shock propagates through the dense CSM, the cool dense shell (CDS) that develops at the SN-CSM interface will create an optically thick barrier that masks the inner high-velocity ejecta. Once the presumed “edge” of the dense CSM envelope is reached, the CDS should rapidly expand and become optically thin. By this time, if the inner ejecta have already cooled below the recombination temperature of hydrogen (~ 6000 K), the explosion should quickly become transparent to the observer, resulting in a rapid drop in continuum flux, and a fast transition into the nebular phase. Since the radiative energy of the inner ejecta is dominated by the thermalization of radioactively generated photons, a sufficiently low mass of radioactive ^{56}Ni could potentially result in such a scenario by allowing the interior to rapidly cool and become transparent before the CDS reaches the edge of the CSM and thins out. Low ^{56}Ni mass is also consistent with the small velocity widths of the emission lines observed during the nebular phases of SNe 2011ht, 1994W, and 2009kn (Maguire et al. 2012). We demonstrate below that the late-time luminosity of SN 2011ht also implies a low mass of radioactive ^{56}Ni synthesized in the explosion.

4.2 Low ^{56}Ni Mass

The decay tails of SNe 2011ht, 1994W, and 2009kn are faint and imply a relatively low yield of ^{56}Ni compared with other known SNe II (Smartt et al. 2009). Since radioactivity provides thermal energy to the ejecta, a larger synthesized mass of ^{56}Ni will not only result in a brighter decay tail in the late-time light curve, but also extend the hydrogen recombination time scale, resulting in a shallower plateau edge and smoother transition into the nebular phase, as exhibited by the light curve of SN 1987A included in Figure 3. SNe that yield a small ^{56}Ni mass exhibit the faintest decay tails and the sharpest plateau edges (e.g., see Elmhamdi et al. 2003). Thus, SNe 2011ht, 1994W, and 2009kn appear fully consistent with relatively low ^{56}Ni -yield core-collapse explosions in all respects.

According to Sutherland & Wheeler (1984), the relationship between the bolometric luminosity of the decay tail and the total mass of ^{56}Ni can be expressed as

$$L = 1.42 \times 10^{43} \text{ erg s}^{-1} e^{-t/111 \text{ days}} M_{\text{Ni}}/M_{\odot}, \quad (2)$$

assuming 100% γ -ray deposition efficiency into the SN envelope. For the moment, let us assume that the light-curve tail of SN 2011ht is dominated by ^{56}Co decay, ignoring potential contribution from residual CSM interaction at late times. The pseudo-bolometric values we derived via SED integration imply a total luminosity of $L_{\text{bol}} = 1.9 \times 10^{40} \text{ erg s}^{-1}$ for SN 2011ht on day 166, recalling that the SED was constructed using the IR measurements from Humphreys et al. (2012) on day 166 with our interpolated optical photometry on the same day. This would imply a ^{56}Ni mass of $\sim 0.006 M_{\odot}$ using Equation 2.

The uncertainty in our ^{56}Ni mass estimate is difficult to ascertain, since we interpolated the optical light curve between our measurements on days 141 and 203. Furthermore, as indicated by our analysis on SN 1987A, which we performed as a check on our method for measuring the pseudo-bolometric luminosity via SED integration, the results underestimated the true bolometric luminosity by $\sim 20\%$ dur-

ing the nebular phase, which would imply that the ^{56}Ni mass of SN 2011ht is probably closer to $0.007\text{--}0.008 M_{\odot}$. However, this reasoning does not account for potential differences between the SEDs of SN 2011ht and SN 1987A. Finally, residual emission from CSM interaction could contribute to the late-time luminosity. Thus, we conclude conservatively that the ^{56}Ni mass of SN 2011ht lies in the range of $0.006\text{--}0.01 M_{\odot}$. Despite the large uncertainty, we can state with confidence that the range of likely values for the ^{56}Ni mass occupies the low end of the range exhibited by SNe II-P (Turatto et al. 1990; Sollerman 2002; Nadyozhin 2003; Smartt et al. 2009), which has important implications that will be discussed below.

One can also estimate the ^{56}Ni mass by direct comparison of decay-tail luminosity to that of the nearby SN 1987A, which provides a reliable benchmark, owing to its well-constrained distance and luminosity. The mass of ^{56}Ni produced by SN 1987A is $\sim 0.07 M_{\odot}$ (Suntzeff & Bouchet 1990). The luminosity of SN 1987A on day 203 was $1.6 \times 10^{41} \text{ erg s}^{-1}$ (Suntzeff et al. 1991). By direct comparison, the luminosity ratio of 0.09 also implies an initial ^{56}Ni mass of $0.006 M_{\odot}$ for SN 2011ht (using the pseudo-bolometric luminosity), consistent with the value from the method of Sutherland & Wheeler (1984). The SN 1987A comparison method was used by Kankare et al. (2012) to estimate a value of $0.023 M_{\odot}$ for SN 2009kn, which was regarded as a lower limit, since the shallower decline rate for this SN indicates the likelihood that persistent CSM interaction continued well into the nebular phase and thus contributed to the late-time bolometric luminosity. Our analysis on SN 2009kn data yields a ^{56}Ni mass consistent with the results of Kankare et al. (2012). Note that in this analysis we assumed the explosion date is the discovery date. We expect that the uncertainty in explosion date for SN 2011ht is likely to be less than 1–2 weeks, since the early UV rise was observed by Roming et al. (2012). A two-week difference would raise the derived ^{56}Ni mass by only 14%, which does not change our conclusion that the ^{56}Ni yield of SN 2011ht is relatively low compared with other core-collapse SNe.

Had we not considered the total optical-IR SED luminosity of SN 2011ht, and instead only used the optical photometry, we would have significantly underestimated the luminosity and, hence, the ^{56}Ni mass. For example, using its absolute magnitude of $M_V = -10.67$ mag on day 203 and adopting a bolometric correction of -0.45 mag for the nebular phase (Bersten & Hamuy 2009), the total luminosity calculated for day 203 would be $5.7 \times 10^{39} \text{ erg s}^{-1}$, implying a factor of 4–5 lower ^{56}Ni mass of $2.4 \times 10^{-3} M_{\odot}$. The underestimated value matches the *lower* end of the range estimated for SN 1994W by Sollerman et al. (1998), who did not have IR measurements at their disposal. Thus, the true ^{56}Ni mass of SN 1994W, if its infrared decay tail properties are similar to SN 2011ht, could be closer to the *upper* end of their derived range ($0.015 M_{\odot}$), for which they considered dust as a potential cause for the unusually steep late-time decline of the optical light curve.

4.3 The Possible Influence of Dust

For SN 1994W, dust formation could have been more tightly constrained if multi-band optical and IR coverage had been obtained at late times. For SN 2011ht, we were fortunate to

have obtained multi-band optical measurements during the nebular phase, which can be combined with the late-time infrared measurements of SN 2011ht reported by Humphreys et al. (2012). The IR data, included in Figure 2, unambiguously demonstrate that substantial flux has shifted into the IR after the plateau phase, and this has been attributed to the formation of dust. However, if the steep optical decline were caused by extinction from such dust, then we might have expected substantial reddening to be observed in the $V - R$ and $V - I$ colors between days 141 and 203. As shown in Figure 2, no such reddening is observed after the plateau phase ends. In fact, the colors appear to flatten out and become slightly bluer, probably because the continuum during the end of the plateau, which exhibited strong line blanketing at the blue end of the spectrum, has dropped out almost completely by day 147.

However, the photometric data are perhaps a bit too sparse at late times to justify making any definitive conclusions about the influence of dust and increasing extinction. However, the late-time luminosity ratio of $H\alpha$ and $H\beta$ emission, shown in Figure 8, does appear to be consistent with increasing reddening, as the last $H\beta$ measurement after day 200 deviates from $H\alpha$ more extremely than for earlier epochs. Alternatively, in the optically thin regime, collisional excitation can result in significant deviations from Case B recombination, which will also result in a decreasing $H\beta$ luminosity; this could be important for the nebular phase. We note that if extinction by dust is important for $H\alpha$, then the estimated CSM wind-density parameters that are based on the luminosity of this line could be significantly underestimated for SN 2011ht.

In conclusion, although the cause of the steep optical decline of SN 2011ht during the nebular decay tail remains unclear, the hypothesis of dust formation is hard to rule out. The steep optical decline during the nebular phase could likely to be the result of the absorption and thermal reprocessing of photons. Such dust could have condensed following the steep drop in luminosity after the plateau, although the rapid time scale over which grains would have had to grow is difficult to reconcile (Humphreys et al. 2012). Whatever the case, the properties of SNe 2011ht, 1994W, and 2009kn underscore the importance of obtaining IR photometry to accompany optical measurements during both the plateau phase and later nebular phases, so that the full bolometric luminosity can be precisely estimated and the possible influence of dust can be realized.

4.4 The Nature of the Explosion and the Progenitor

The results of our observations and analysis suggest a low ^{56}Ni mass of 0.006–0.01 M_{\odot} for SN 2011ht, and this has important implications for the nature of the progenitor. ^{56}Ni yields this low could result from the lowest-mass stars believed to be capable of undergoing core collapse. Stars with initial masses of 8–10 M_{\odot} are not thought to produce an Fe core. Instead, they are thought to end their lives as super-asymptotic-giant-branch (SAGB) stars which develop electron-degenerate O-Ne-Mg cores (Barkat 1974; Nomoto 1984). The favored core-collapse mechanism in this case is electron capture onto ^{24}Mg and ^{20}Ne , which triggers collapse before the onset of explosive O burning (Miyaji et al. 1980).

Owing to the low overall mass and the neutron richness of the ejecta, nucleosynthesis models for electron-capture SNe predict low ^{56}Ni yields, perhaps as small as 0.002 M_{\odot} (Wanajo et al. 2009), but more conservatively $< 0.015 M_{\odot}$ (Kitaura et al. 2006). The model yields for 8–10 M_{\odot} stars appear to be consistent with the volume-limited sample of relatively nearby core-collapse SNe that have identified progenitors and constrained initial masses (Smartt et al. 2009).

The light curves of SN 2011ht, 1994W, 2009kn, and 2005cl bear some resemblance to other interacting SNe which have been considered viable candidates for electron-capture SNe. The low-luminosity SN 2005cs, whose light curve is shown in Figure 3, exhibited a similarly steep plateau edge and a subluminous decline, implying a very low ^{56}Ni mass of $3 \times 10^{-3} M_{\odot}$ (Pastorello et al. 2009). The progenitor had an estimated mass of $9_{-2}^{+3} M_{\odot}$, derived from pre-SN images of its nearby host galaxy M51 (Maund et al. 2005). Based on these properties, SN 2005cs was considered a viable candidate for an electron-capture SN. However, the IR colors of the progenitor derived from archival *HST* images, appeared inconsistent with those of an SAGB star (Eldridge et al. 2007), which is the expected progenitor of such an explosion.

Other candidates for electron-capture SNe from SAGB progenitors are SN 2008S (Prieto et al. 2008; Botticella et al. 2009) and SN 2007od (Inserra et al. 2011). SN 2008S exhibited a spectral morphology and evolution similar to SNe 2011ht, 1994W, and 2009kn, indicative of CSM interaction. Moreover, SED modeling of its strong mid-IR excess indicated that the CSM likely consists of multiple dusty optically thick shells. Although the light curve plateau of SN 2008S did not exhibit as steep an edge as SN 2011ht, the derived ^{56}Ni mass was nonetheless a very low $\sim 10^{-3} M_{\odot}$. Evidence in support of an SAGB progenitor for SN 2008S is also strong in this case, owing to the detection of the progenitor star in archival mid-infrared images from the *Spitzer Space Telescope*, which exhibited an SED consistent with this interpretation (Thompson et al. 2009; Prieto et al. 2009). Finally, the light curve of SN 2007od exhibited a well-defined plateau with a duration of 100–120 days, similar to that of SN 2011ht. However, this object’s spectral evolution during the plateau exhibited very broad lines typical of normal SNe II-P, in contrast to the narrow-lined spectra exhibited by SN 2011ht and SN 2008S. Although evidence for CSM interaction did appear in the late spectra of SN 2007od, in the form of a boxy multi-peaked $H\alpha$ line (Inserra et al. 2011), the persistence of broad lines throughout its entire evolution imply that an optically-thick shell capable of masking the inner high-velocity SN ejecta never developed, perhaps because the CSM mass and density was relatively low, or because of an aspherical geometry for the CSM.

It seems plausible that SN 2011ht could be an explosion from an 8–10 M_{\odot} progenitor, as already suggest for SN 2009kn by Kankare et al. (2012), although with more luminous CSM interaction. The nebular phase spectra might also be consistent with this interpretation. Specifically, the feeble emission from [O I] $\lambda 6303$, which is weak in SN 2011ht and not detected in SN 2009kn or SN 1994W, favors a relatively low-mass progenitor, as indicated by Dessart et al. (2010).

If SNe 2011ht, 1994W, and 2009kn did arise from 8–10

M_{\odot} progenitors, then the minor differences between their photometric and spectroscopic evolution could potentially be the result of variations within the masses and radial density profiles of their CSM envelopes, in addition to differences in explosion energy. In the case of SN 1994W, which we believe has CSM parameters similar to SN 2011ht, Chugai et al. (2001) estimated a CSM mass of $0.3 M_{\odot}$ with a radius of $R \sim 300\text{AU}$, and an approximate volume density of $n \sim 1 \times 10^9 \text{ cm}^{-3}$. In the case of SN 2008S, SED modeling indicates a significantly lower mass and density CSM of $M = 10^{-3} M_{\odot}$ and $n = 3 \times 10^7 \text{ cm}^{-3}$ (Prieto et al. 2008), which results in less efficient conversion of SN kinetic energy into optical light, and, hence, a lower peak luminosity for the light curve.

Indeed, the CSM configurations of electron-capture progenitor AGB stars are potentially very diverse, exhibiting a large variety at the time of core collapse. Depending on factors such as metallicity (Pumo et al. 2009), possible activity from He or C burning flashes, or perhaps core-O or Ne flashes. For SN 2011ht, the ejection of CSM in the several years before core collapse could have resulted from explosive instabilities that occur during the late nuclear burning stages and/or SAGB winds (e.g., Poelarends et al. 2008, and references therein). However, the $500\text{--}800 \text{ km s}^{-1}$ velocity of the P-Cygni absorption components of SNe 2011ht are significantly faster than the observed wind velocities of SAGB stars ($\sim 10 \text{ km s}^{-1}$). Still, there is no particular reason to suspect that eruptive pre-SN mass loss from final nuclear flashes should share the low outflow velocities of earlier and more steady SAGB winds.

As an alternative to the possibility of low-mass progenitors and electron-capture SNe, a low ^{56}Ni yield explosion can result if a substantial fraction of the inner core ejecta does not achieve the escape velocity necessary for a successful explosion and thus falls back onto the compact remnant, perhaps accreting onto a neutron star or descending into a black hole (Zampieri et al. 2003). If this is the case, then the progenitors of SN 2011ht and its kin could have been substantially more massive than $8\text{--}10 M_{\odot}$, perhaps having initial masses of $30 M_{\odot}$ or more (Fryer 1999). Consider the case of the jet-powered SN 2010jp, which has been suggested to possibly mark the formation of a black hole (Smith et al. 2012b). This SN II_n exhibited a steeply declining decay tail with a low overall luminosity, which constrained the ^{56}Ni mass to $< 0.003 M_{\odot}$. Black hole formation is likely preceded by substantial fallback of SN ejecta, so low ^{56}Ni masses are to be expected in such a scenario.

There has also been the suggestion that SN 2011ht may represent a non-terminal event. Dessart et al. (2009) suggested that SN 1994W could have resulted from the interaction of colliding circumstellar shells that were ejected from consecutive mass eruptions, where the more recent ejection has a higher velocity and catches up with the slower outer shell, creating a luminous collision by conversion of kinetic energy into UV-optical-IR light. If SN 2011ht was the result of an LBV eruption, however, it would be a rather remarkable set of coincidences for the end of the plateau phase to occur at ~ 120 days, which is a very typical time scale for SNe II-P, and for the late-time bolometric decline to be consistent with the ^{56}Co decay rate. The uncanny spectroscopic and photometric similarity of SN 2011ht and SN 1994W to SN 2009kn and SN 2005cl, which were almost certainly bona

fide core-collapse events, would also be a rather remarkable coincidence.

Arguments in favor of the nonterminal LBV scenario (e.g., Humphreys et al. 2012) are based on a plausibility argument, and thus provide insufficient evidence against core collapse. The lack of observational signatures from high-velocity material in the spectra of SNe 2011ht, 1994W, and 2009kn can be explained by the presence of an optically thick CDS that remains present during the entire plateau phase, which masked emission from inner high-velocity material. A similar process was invoked to explain the spectrum of the luminous SN 2006gy (Smith et al. 2010), which shares many spectral similarities with these SNe. By the time the CDS thinned out, the explosion could have cooled and become transparent, never revealing the observational signature of high-velocity ejecta. As we pointed out earlier, the exceptionally low ^{56}Ni masses derived for SN 2011ht, SN 1994W, and, to a lesser extent, SN 2009kn, could allow for such rapid cooling and optical thinning of the ejecta, as the radioactive energy source was weak in these cases compared with normal SNe II. Finally, the interpretation of the SN 2011ht spectrum as the result of a radiatively driven “opaque wind” is not physically plausible. Assuming that Thomson scattering dominates the optical depth ($\kappa_e = 0.34$), the SN 2011ht peak luminosity of $L_{\text{peak}} = (5 \pm 2) \times 10^{42} \text{ erg s}^{-1}$ would imply an Eddington factor of $\Gamma = (\kappa_e L) / 4\pi G M c \approx 1000$, which would undoubtedly result in explosive mass loss, not a wind, as suggested by Humphreys et al. (2012).

The only reliable means to observationally discriminate between the possibility of electron-capture SNe, a fallback scenario, or surviving LBVs would be the detection of the progenitor from deep pre-SN space-based images of the host galaxy, or an upper limit in the case of the electron-capture scenario. Unfortunately, pre-existing SDSS images of the SN 2011ht host, UGC 4560, do not place firm constraints on the nature of the progenitor, other than the fact that it could not be a progenitor as luminous as η Car (Roming et al. 2012). However, LBVs on the fainter end of the distribution (Smith, Vink, & de Koter 2004) may be possible. Still, scenarios that produce multiple massive shell ejections, such as the pulsational pair instability (Woosley et al. 2007), require extremely massive stars ($> 90 M_{\odot}$), which would also be extremely luminous and can therefore be ruled out. This scenario would also seem unlikely to produce three SNe having such similar observational characteristics.

5 CONCLUSIONS

We have presented extensive photometric and spectroscopic coverage of SN 2011ht. Our data complement those published by Roming et al. (2012) and Humphreys et al. (2012), but we arrive at somewhat different conclusions. This SN II_n shares with SN 1994W and SN 2009kn an unusual combination of properties, including a well-defined and abruptly ending plateau phase dominated by CSM interaction, and low yields of ^{56}Ni . The results of our analysis, particularly the late-time bolometric decline being consistent with the ^{56}Co decay rate, supports the hypothesis that SN 2011ht, like SN 2009kn, was a core-collapse SN, and not the result of a super-Eddington wind. The more exotic scenario of multiple colliding LBV shells (Dessart et al. 2009) is a

little more difficult to firmly rule out, although there is no reason why such a scenario should produce the plateau duration of ~ 120 days, which is so common among SNe II-P (Hamuy 2003), or a late-time decline that is consistent with ^{56}Co decay. The most likely scenario is that SN 2011ht was a bona fide core-collapse SN that produced a low ^{56}Ni yield and exploded into dense CSM. Its discovery marks the third or fourth addition to an unusual group of SNe II_n, including SN 1994W and SN 2009kn, and perhaps SN 2005cl. We argue that this justifies the designation of a new subclass of SNe exhibiting Type II_n spectra, well-defined plateau light curves, and faint decay tails, which we propose be Type II_n-P. The low synthesized mass of ^{56}Ni for these events highlights the possibility that they are either the result of electron-capture SNe from 8–10 M_{\odot} progenitors, or explosions which experienced substantial fallback of their inner metal-rich ejecta. Additional members of the Type II_n-P class will undoubtedly emerge from future all-sky surveys, such as Pan-STARRS, the Large Synoptic Survey Telescope (LSST), and SkyMapper, and will enable the physical nature of these explosions to be elucidated more completely. Statistics for their rates and host-galaxy environments may also help discriminate between the two likely origins.

ACKNOWLEDGMENTS

This work is based in part on observations made at the the MMT Observatory, a joint facility of the Smithsonian Institution and the University of Arizona, and at the Lick Observatory, which is owned and operated by the University of California. Some of the data presented herein were obtained at the W. M. Keck Observatory, which is operated as a scientific partnership among the California Institute of Technology, the University of California, and NASA; the observatory was made possible by the generous financial support of the W. M. Keck Foundation. Infrared data herein were obtained using PAIRITEL, which is operated by the Smithsonian Astrophysical Observatory (SAO) and was made possible by a grant from the Harvard University Milton Fund, the camera loan from the University of Virginia, and the continued support of the SAO and UC Berkeley. We thank the staffs at these observatories for their efficient assistance. We are grateful to P. E. Nugent, D. Cohen, B. Y. Choi, M. Ellison, M. Mason, A. Wilkins, P. Blanchard, M. T. Kandrashoff, and O. Nayak for their help with observations at Keck and Lick. We also thank A. A. Miller, D. Starr, and C. Blake for facilitating PAIRITEL data contributions. E. Kankare kindly provided several epochs of spectra of SN 2009kn for our comparison. The supernova research of A.V.F.'s group at U.C. Berkeley is supported by Gary & Cynthia Bengier, the Richard & Rhoda Goldman Fund, the Christopher R. Redlich Fund, the TABASGO Foundation, and NSF grants AST-0908886 and AST-1211916.

REFERENCES

- Barkat, Z. 1971, *ApJ*, 163, 433
- Begelman, M. C., & Sarazin, C. L. 1986, *ApJ*, 302, L59
- Bersten, M. C., & Hamuy, M. 2009, *ApJ*, 701, 200
- Bloom, J. S., Starr, D. L., Blake, C. H., Skrutskie, M. F., & Falco, E. E. 2006, in *Astronomical Data Analysis Software and Systems XV*, ed. C. Gabriel, et al. (SF: ASP, vol. 351), 751
- Botticella, M. T., Pastorello, A., Smartt, S. J., et al. 2009, *MNRAS*, 398, 1041
- Bouchet, P., Phillips, M. M., Suntzeff, N. B., Gouffes, C., Hanuschik, R. W. and Wooden, D. H. 1991, *A&A*, 245, 490
- Bowen, D. V., Roth, K. C., Meyer, D. M., & Blades, J. C. 2000, *ApJ*, 536, 225
- Catchpole, R. M., Menzies, J. W., Monk, A. S., et al. 1987, *MNRAS*, 229, 15P
- Catchpole, R. M., Whitelock, P. A., Feast, M. W., et al. 1988, *MNRAS*, 231, 75P
- Chugai, N. N. 1990, *Sov. Astron. Let.*, 16, 457
- Chugai, N. N. 2001, *MNRAS*, 326, 1448
- Chugai, N. N. 2009, *MNRAS*, 400, 866
- Chugai, N. N., Blinnikov, S. I., Cumming, R. J., et al. 2004, *MNRAS*, 352, 1213
- Dessart, L., Hillier, D. J., Gezari, S., Basa, S., & Matheson, T. 2009, *MNRAS*, 394, 21
- Dessart, L., Livne, E., & Waldman, R. 2010, *MNRAS*, 408, 827
- Eldridge, J. J., Mattila, S., & Smartt, S. J. 2007, *MNRAS*, 376, L52
- Imhamdi, A., Chugai, N. N., & Danziger, I. J. 2003, *A&A*, 404, 1077
- Elmhamdi, A., Tsvetkov, D., Danziger, I. J., & Kordi, A. 2011, *ApJ*, 731, 129
- Fesen, R. A., & Becker, R. H. 1990, *ApJ*, 351, 437
- Filippenko, A. V. 1982, *PASP*, 94, 715
- Filippenko, A. V. 1997, *ARAA*, 35, 309
- Filippenko, A. V., & Sargent, W. L. W. 1985, *Nature*, 316, 407
- Foley, R. J., Smith, N., Ganeshalingam, M., Li, W., Chornock, R., and Filippenko, A. V. 2007, *ApJL*, 657, L105
- Fryer, C. L. 1999, *ApJ*, 522, 413
- Gal-Yam, A., & Leonard, D. C. 2009, *Nature*, 458, 865
- Hamuy, M. 2003, *ApJ*, 582, 905
- Hamuy, M., Suntzeff, N. B., Bravo, J., & Phillips, M. M. 1990, *PASP*, 102, 888
- Humphreys, R. M., Davidson, K. Jones, T. J., Pogge, R. W., Grammer, S. H., Prieto, J. L. and Pritchard, T. A. 2012, *ApJ*, 760, 93
- Insera, C., Turatto, M., Pastorello, A., et al. 2011, *MNRAS*, 417, 261
- Kankare, E., Ergon, M., Bufano, F., et al. 2012, *MNRAS*, 424, 855
- Kiewe, M., Gal-Yam, A., Arcavi, I., et al. 2012, *ApJ*, 744, 10
- Kitaura, F. S., Janka, H.-T., & Hillebrandt, W. 2006, *A&A*, 450, 345
- Kochanek, C. S., Szczygiel, D. M., & Stanek, K. Z. 2011, *ApJ*, 737, 76
- Li, W., Leaman, J., Chornock, R., et al. 2011, *MNRAS*, 412, 1441
- Maguire, K., Jerkstrand, A., Smartt, S. J., et al. 2012, *MNRAS*, 420, 3451
- Maund, J. R., Smartt, S. J., & Danziger, I. J. 2005, *MNRAS*, 364, L33
- Mauerhan, J., & Smith, N. 2012, *MNRAS*, 424, 2659
- Mauerhan, J. C., Smith, N., Filippenko, A. V., et al. 2012, *arXiv:1209.6320*
- MacFadyen, A. I., & Woosley, S. E. 1999, *ApJ*, 524, 262
- Menzies, J. W., Catchpole, R. M., van Vuuren, G., et al. 1987, *MNRAS*, 227, 39P
- Milislavljevic, D., Fesen, R. A., Chevalier, R. A., Kirshner, R. P., Challis, P., and Turatto, M. 2012, *ApJ*, 751, 25
- Miller J. S., & Stone, R. P. S. 1993, *Lick Obs. Tech. Rep. 66* (Santa Cruz: Lick Obs.)
- Miyaji, S., Nomoto, K., Yokoi, K., & Sugimoto, D. 1980, *PASJ*, 32, 303
- Nadyozhin, D. K. 2003, *MNRAS*, 346, 97
- Nomoto, K. 1984, *ApJ*, 277, 791

- Oke, J. B., Cohen, J. G., Carr, M., et al. 1995, *PASP*, 107, 375
- Pastorello, A., Sauer, D., Taubenberger, S., et al. 2006, *MNRAS*, 370, 1752
- Pastorello, A., Stanishev, V., Smartt, S. J., & Fraser, M. 2011, *CBET*, 2851
- Pastorello, A., Valenti, S., Zampieri, L., et al. 2009, *MNRAS*, 394, 2266
- Pastorello, A., Zampieri, L., Turatto, M., et al. 2004, *MNRAS*, 347, 74
- Poelarends, A. J. T., Herwig, F., Langer, N., & Heger, A. 2008, *ApJ*, 675, 614
- Pooley, D. 2012, *ATEL*, 4062
- Prieto, J. L., McMillan, R., Bakos, G., & Grennan, D. 2011, *Central Bureau Electronic Telegrams*, 2903, 1
- Prieto, J. L., Kistler, M. D., Thompson, T. A., et al. 2008, *ApJL*, 681, L9
- Prieto, J. L., Sellgren, K., Thompson, T. A., & Kochanek, C. S. 2009, *ApJ*, 705, 1425
- Pumo, M. L., Turatto, M., Botticella, M. T., et al. 2009, *ApJL*, 705, L138
- Roming, P., 2011, *ATEL*, 3690
- Roming, P. W. A., Pritchard, T. A., Prieto, J. L., et al. 2012, *ApJ*, 751, 92
- Schlegel, E. M. 1990, *MNRAS*, 244, 269
- ilverman, J. M., Foley, R. J., Filippenko, A. V., et al. 2012, *MNRAS*, 425, 1789
- Smartt, S. J., Eldridge, J. J., Crockett, R. M., & Maund, J. R. 2009, *MNRAS*, 395, 1409
- Smith, N., Chornock, R., Li, W., et al. 2008, *ApJ*, 686, 467
- Smith, N., Li, W., Filippenko, A. V., & Chornock, R. 2011b, *MNRAS*, 412, 1522
- Smith, N., Li, W., Silverman, J. M., Ganeshalingam, M., & Filippenko, A. V. 2011a, *MNRAS*, 415, 773
- Smith, N., Li, W., Foley, R. J., et al. 2007, *ApJ*, 666, 1116
- Smith, N., Mauerhan, J. C., Silverman, J. M., Ganeshalingam, M., Filippenko, A. V., Cenko, S. B., Clubb, K. I., and Kandrashoff, M. T. 2012a, *MNRAS*, 426, 1905
- Smith, N., Cenko, S. B., Butler, N., et al. 2012b, *MNRAS*, 420, 1135
- Smith, N., & Owocki, S. P. 2006, *ApJ*, 645, L45
- Smith, N., Silverman, J. M., Chornock, R., et al. 2009, *ApJ*, 695, 1334
- Smith, N., Chornock, R., Silverman, J. M., Filippenko, A. V., & Foley, R. J. 2010, *ApJ*, 709, 856
- Smith, N., Vink, J. S., & de Koter, A. 2004, *ApJ*, 615, 475
- Sollerman, J. 2002, *NewAR*, 46, 493
- Sollerman, J., Cumming, R. J., & Lundqvist, P. 1998, *ApJ*, 493, 933
- Suntzeff, N. B., & Bouchet, P. 1990, *AJ*, 99, 650
- Suntzeff, N. B., Phillips, M. M., Depoy, D. L., Elias, J. H., & Walker, A. R. 1991, *AJ*, 102, 1118
- Sutherland, P. G., & Wheeler, J. C. 1984, *ApJ*, 280, 282
- Thompson, T. A., Prieto, J. L., Stanek, K. Z., Kistler, M. D., Beacom, J. F., and Kochanek, C. S. 2009, *ApJ*, 705, 1364
- Turatto, M., Cappellaro, E., Barbon, R., della Valle, M., Ortolani, S., and Rosino, L. 1990, *AJ*, 100, 771
- Turatto, M., Mazzali, P. A., Young, T. R., et al. 1998, *ApJL*, 498, L129
- Van Dyk, S. D., Peng, C. Y., King, J. Y., Filippenko, A. V., Treffers, R. R., Li, W., and Richmond, M. W. 2000, *PASP*, 112, 1532
- Wanajo, S., Nomoto, K., Janka, H.-T., Kitaura, F. S., Müller, B. 2009, *ApJ*, 695, 208
- Weiler, K. W., van Dyk, S. D., Discenna, J. L., Panagia, N., & Sramek, R. A. 1991, *ApJ*, 380, 161
- Woosley, S. E., Blinnikov, S., & Heger, A. 2007, *Nature*, 450, 390
- Woosley, S. E., & Weaver, T. A. 1980, *ApJ*, 238, 1017
- Yaron, O., & Gal-Yam, A. 2012, *PASP*, 124, 668
- Zampieri, L., Pastorello, A., Turatto, M., Cappellaro, E., Benetti, S., Altavilla, G., Mazzali, P., and Hamuy, M. 2003, *MNRAS*, 338, 711